Lab on a Chip

PAPER

View Article Online
View Journal

Cite this: DOI: 10.1039/c9lc00267g

Magnetic microboats for floating, stiffness tunable, air–liquid interface epithelial cultures†

Arvind Chandrasekaran, ‡[a] Sonya Kouthouridis,[a] Wontae Lee,[a] Nicholas Lin,[a] Zhenwei Ma,[a] Mark J. Turner,[b] John W. Hanrahan[bc] and Christopher Moraes *acde

To study respiratory diseases, *in vitro* airway epithelial models are commonly implemented by culturing airway cells on a porous surface at an air–liquid interface (ALI). However, these surfaces are often supraphysiologically stiff, which is known to affect the organization, maturation, and responses of cells to potential therapies in other biological culture models. While it is possible to culture cells on soft hydrogel substrates at an air–liquid interface, these techniques are challenging to implement particularly in high-throughput applications which require robust and repetitive material handling procedures. To address these two limitations and characterize epithelial cultures on substrates of varying stiffness at the ALI, we developed a novel "lung-on-a-boat", in which stiffness-tuneable hydrogels are integrated into the bottoms of polymeric microstructures, which normally float at the air–liquid interface. An embedded magnetic material can be used to sink the boat on demand when a magnetic field is applied, enabling reliable transition between submerged and ALI culture. In this work, we prototype a functional ALI microboat platform, with integrated stiffness-tunable polyacrylamide hydrogel surfaces, and validate the use of this technology with a model epithelial cell line. We verify sufficient transport through the hydrogel base to maintain cell viability and stimulate cultures, using a model nanoparticle with known toxicity. We then demonstrate significant morphological and functional effects on epithelial barrier formation, suggesting that substrate stiffness is an important parameter to consider in the design of *in vitro* epithelial ALI models for drug discovery and fundamental research.

Received 21st March 2019,
Accepted 14th July 2019

DOI: 10.1039/c9lc00267g

rsc.li/loc

1. Introduction

Cells in the human airway epithelium are responsible for the genesis, chronicity and severity of several respiratory diseases including cystic fibrosis (CF), chronic obstructive pulmonary disorder (COPD), and asthma.[1–4] *In vitro* cell culture models are of critical importance in understanding and addressing these diseases.[5–7] These models require culturing cells at an air–liquid interface (ALI), which is now a well-established and accepted technique for driving realistic cell morphology and function of the *in vivo* airway epithelium.[8,9] The ALI culture method requires epithelial cells to be grown on a porous membrane, and exposed to air at their apical surfaces while maintaining nutrient uptake from the basolateral side. The ALI is most commonly implemented using commercially-available Transwell® inserts,[10] in which cells are grown on a track-etched porous polymer membrane mounted in a plastic frame and cultured in a multi-well plate. Carefully removing media from the apical cell surface after they reach confluence initiates ALI culture (Fig. 1A).

The ALI culture format itself presents significant handling challenges, particularly for higher-throughput applications that would require automation. Multiple object- and liquid-manipulation steps are required to submerge and then return the culture to ALI. This is often required for repetitive drug dosing protocols, or when monitoring functional epithelial barrier integrity using techniques such as trans-epithelial electrical resistance (TEER).[11,12] The need to perform these steps sequentially on the same cultures requires repeated transitions between submerged and ALI conditions (summarized in Fig. 1B). Even though automation is possible, the liquid handling steps must still be performed accurately and precisely to ensure that all fluid is drawn out of the apical chamber without accidentally damaging the delicate layer of cells

[a] *Department of Chemical Engineering, McGill University, Montreal, Canada. E-mail: chris.moraes@mcgill.ca*
[b] *Department of Physiology, McGill University, Montreal, QC, Canada*
[c] *Cystic Fibrosis Translational Research Center, McGill University, Montreal, Canada*
[d] *Department of Biological and Biomedical Engineering, McGill University, Montreal, Canada*
[e] *Goodman Cancer Research Center, McGill University, Montreal, Canada*
† Electronic supplementary information (ESI) available. See DOI: 10.1039/c9lc00267g
‡ Present affiliation: Department of Chemical, Biological and Bio Engineering, North Carolina A&T State University, Greensboro, USA.

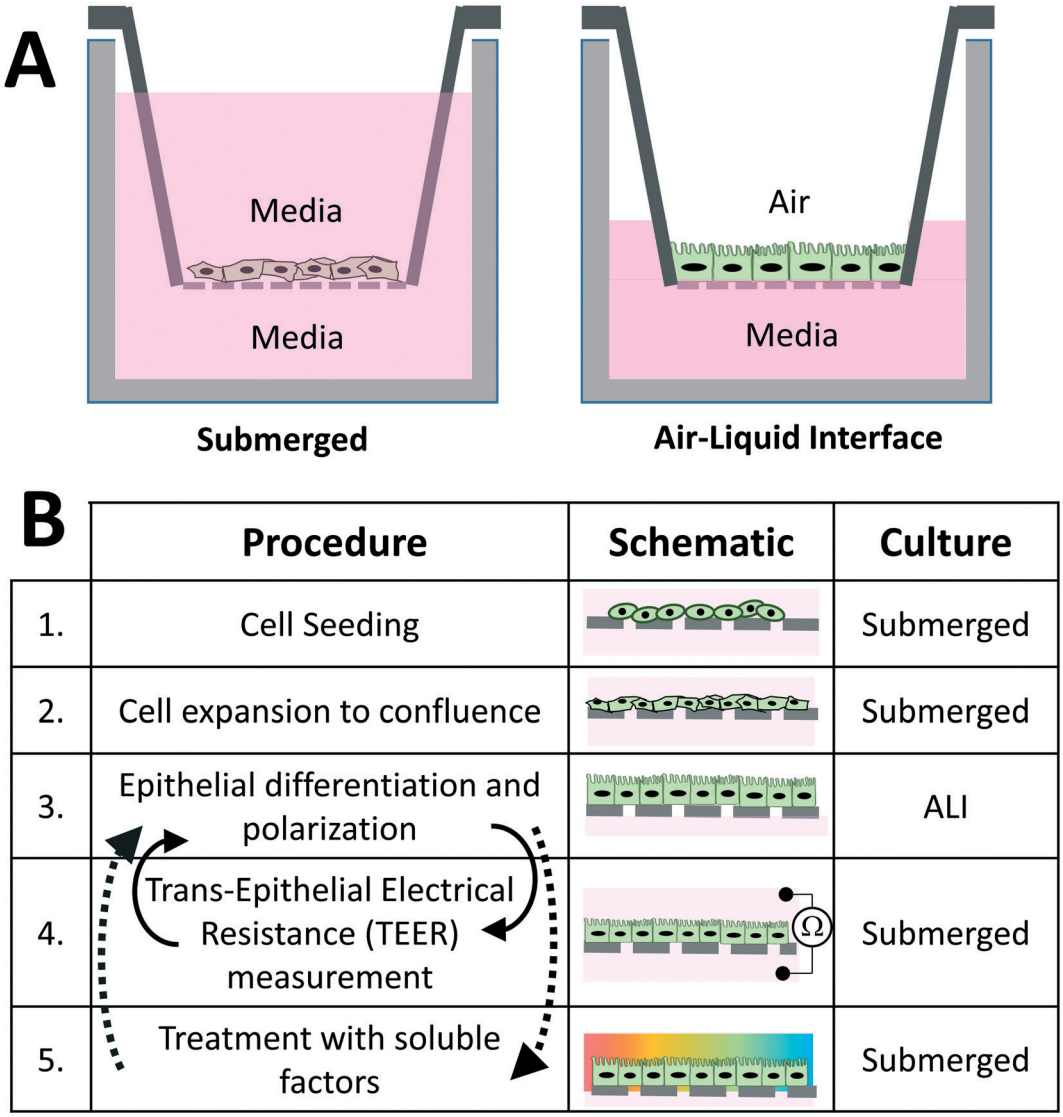

Fig. 1 (A) Schematic illustration of the airway epithelial cell culture under submerged and air–liquid interface (ALI) culture conditions, which is commonly used to establish a realistic epithelium when culturing lung epithelial cells *in vitro*. (B). Establishing air–liquid interface cultures requires an initial seeding and expansion step, and repeated transitions between ALI and submerged culture during differentiation, treatment and analysis.

with a pipette tip. Even slight damage can invalidate an experiment. These factors make manual culture and automated scale-up beyond 96 well-plate formats extremely challenging.

Microfluidic devices[13–16] or organ-on-a-chip technologies[17] address the liquid handling issues in transitioning between submerged and ALI cultures, and are thus promising strategies to partially reduce the difficulty with ALI cultures. These devices have also recently been integrated with natural hydrogel matrices such as collagen and Matrigel,[18–20] which are sufficiently porous to allow nutrient transport across the basal support structure. However, microfluidic devices remain challenging for non-experts to build and operate, limiting their utility particularly for higher-throughput applications;[21] and natural matrices lack precise control over matrix mechanics.[22] Substrate rigidity or stiffness has now been well-established as a critically important and exquisitely sensitive regulator of cell and tissue function[23–26] particularly in the airway,[27–31] where it is known to affect critically important processes including extracellular matrix deposition,[32] wound healing,[33] and epithelial–mesenchymal transition.[34] Since airways stiffen under disease conditions,[35] incorporating this parameter into ALI cultures to screen therapies for example, could result in more translational or disease-specific findings. Hence, integrating a mechanically-defined hydrogel matrix[23] into an easily-handled and scalable air–liquid interface culture system could be a valuable tool to study airway mechanobiology and implement those findings into the design of disease screening platforms. Although these two core challenges may be individually addressed through various engineered solutions, reliably achieving ALI culture on stiffness-tunable substrates is particularly difficult. The transparent hydrogel makes it difficult to aspirate media

cleanly without touching the cell monolayer; and because epithelial cell adhesion is significantly weaker on soft hydrogels[36] cells are more prone to mechanical damage during liquid aspiration and handling. Moreover, epithelial sheets are mechanically pre-stressed and even small defects can initiate larger zones of damage.[37] Hence, simultaneously addressing these two core challenges requires a redesign of the ALI culture platform to allow for robust, scalable, and mechanically tunable cultures.

Here, we integrate polyacrylamide hydrogels into a redesigned culture platform that allows easy and repeated and on-demand transition between submerged and ALI cultures. Inspired by a concept originally published in the 1970s in which cells are grown at ALI by floating collagen membranes on a liquid surface,[38] we integrated stiffness-tunable polyacrylamide hydrogels into buoyant, free-floating, silicone rings, that rise to the liquid surface to form an ALI, and can be magnetically 'sunk' on demand to allow cell seeding, submersed dosing, and measurement assays. Magnetic submersion and release demonstrated here is rapid and reliable, and does not require precise liquid handling capabilities or equipment to repeatedly transition between submerged and ALI conditions when seeding, culturing, treating or assaying the cultures. The stiffness of the culture platform can be easily tuned across the physiological range of healthy and diseased airway tissue stiffness (1 to 15 kPa)[39] by altering the monomer and crosslinker densities, and the hydrogels within this stiffness range are sufficiently porous to allow transport of test molecules through the basal hydrogel substrate. Using this platform, we demonstrate that substrate stiffness significantly affects the structure of human bronchial epithelial cells under ALI culture in terms of morphology and cell–cell junction formation, suggesting the need for further studies that incorporate mechanically-defined culture conditions for lung cells.

2. Materials and methods

Unless otherwise stated, all cell culture materials and supplies were purchased from Fisher Scientific (Ottawa, ON), and chemicals from Sigma Aldrich (Oakville, ON).

2.1 Fabrication of silicone microboats

Two designs of microboats were fabricated for different purposes. The standard boats described in the main manuscript were used for the majority of experiments and consisted of a simple ring of polydimethylsiloxane (PDMS) with an embedded magnetic wire (Fig. 1). To facilitate TEER measurement a slightly modified microboat format was used, in which a small surface well accommodates standard chopstick electrodes used in TEER measurement (Fig. S2†). The operational principles between the two microboats are the same, and the TEER-compatible boat can be replaced with the standard boat by designing an appropriate TEER measurement clamping system (see Discussion).

To fabricate standard microboats with consistent dimensions, a 1″ × 1″ square plastic mold consisting of an array of circular tapered grooves (4.45 mm diameter, 50 μm tall, 100 μm wide) was fabricated using a benchtop 3D stereolithographic printer (Autodesk, MA; Fig. 2A). To facilitate easy removal of the PDMS from 3D printed parts, molds were spray-coated with ease-release 200 (Mann Release Technologies). For these proof-of-concept experiments, stainless steel fiber ringlets were cut from commercially-available stainless steel scrubbers and held in place in the grooves using a magnet (Fig. 2A). Sylgard 184 PDMS (Dow Corning) was mixed in a standard 10 : 1 monomer to crosslinker mass ratio, degassed and poured onto the plastic mold. To color code the PDMS, store-bought food colouring dye was added to the PDMS mixture. To ensure height control over the produced PDMS rings, a flat polyethylene sheet was placed on top, and the setup was left to cure at 70 °C for 2 hours. The polyethylene sheet was then peeled away, and the PDMS was peeled from the mold. Biopsy punches (6 mm and 3 mm) were then used to remove the PDMS rings using the indented surfaces as a guide.

2.2 Integration of polyacrylamide in PDMS rings

Polyacrylamide gels were grafted onto PDMS surfaces as previously described.[40] Briefly, PDMS was treated with benzophenone (10% w/v) in diluted acetone (65% in water) for 60 seconds, to swell and adsorb benzophenone into the silicone material. The samples were then rinsed with methanol and dried with nitrogen gas. Polyacrylamide prepolymer with acrylamide to bisacrylamide (Bio-Rad) ratios of 7.5/0.24 wt% and 0.1% tetramethylethylenediamine (TEMED; Sigma-Aldrich, T7024) were prepared in a centrifuge tube. 100 μL of freshly-prepared 1% w/v ammonium persulfate (APS) initiator was added to 900 μL of polyacrylamide prepolymer, mixed homogeneously using a vortex mixer and added to the PDMS ring (Fig. 2). PDMS rings were placed on a Rain-X (ITW Global Brands; Houston, TX) treated glass surface, and the prepolymer solution was pipetted into the ring. A Rain-X treated glass coverslip was placed on top of the ring and the setup was allowed to polymerize under UV light for 20 minutes to activate the surface-grafted benzophenone photoinitiator (Fig. 2B). After gelation, microboats were washed three times with phosphate-buffered saline (PBS) and incubated in PBS overnight on a shaker, to leach out any excess toxic benzophenone. Other polyacrylamide formulations were selected from previously published protocols[41] (Table 1), and characterized using shear rheometry.

Polyacrylamide-integrated microboats were sterilized under germicidal UV for 30 minutes. Since native polyacrylamide is non-adherent to cells, the polyacrylamide surface was functionalized with type I collagen using standard crosslinking chemistries. The polyacrylamide surface was treated with 0.2 mg ml^{-1} SulfoSANPAH (Pierce Biotech) under sterile conditions and exposed to a 36 W UV light for 4 minutes. The treated surfaces were then incubated overnight at 4 °C with 0.1 mg mL^{-1} of type I bovine collagen (Advanced Biomatrix, USA), to bind the protein onto the hydrogel surface. Prior to cell seeding, the polyacrylamide substrates were

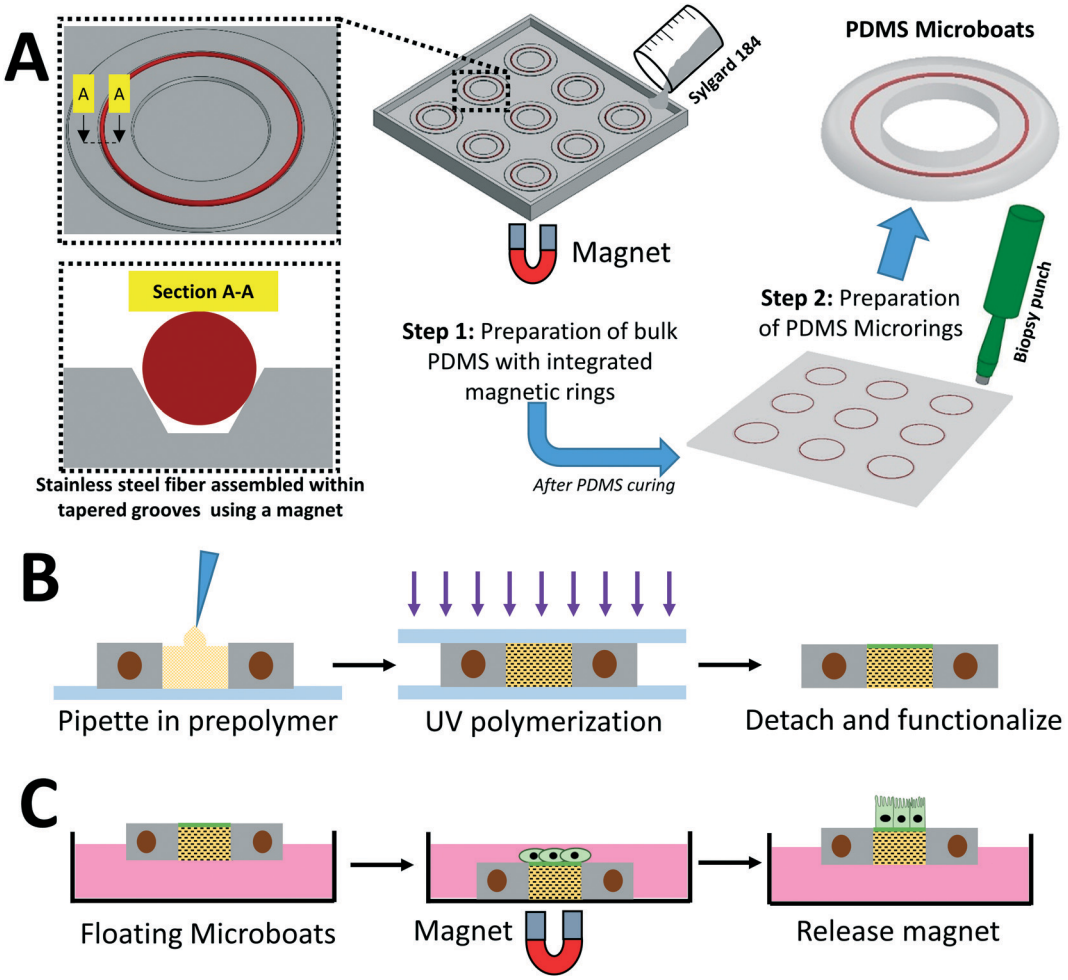

Fig. 2 Overview of device fabrication and operation. (A) To form the PDMS microboats, a 3D printed mold is designed to hold a magnetic fiber (red ring) within a template. PDMS is cast and cured on this surface, and PDMS microboats are punched out with biopsy punches using the raised features as a positioning guide. (B) Polyacrylamide hydrogels are grafted onto the PDMS substrates through a benzophenone initiated UV photografting technique.[40] (C) Ordinarily, devices float at the liquid interface, but can be submerged by placing a strong magnet beneath the culture dish, which rapidly submerges the floating boat, to achieve submerged culture. Releasing the magnet allows the buoyant boat to return to the air–liquid interface.

incubated for 30 minutes with serum-free culture medium to displace PBS from the porous hydrogel.

2.3 Characterization of polyacrylamide hydrogel mechanical stiffness

Mechanical characterization of bulk polyacrylamide hydrogels was performed using a parallel plate, strain-controlled shear rheometer (Anton-Paar, MCR 302). To test the composite polyacrylamide-PDMS samples, 12 mm diameter round coverslips were spin-coated with PDMS at 3000 rpm for 30 s. After curing in a 70 °C oven for two hours, the glass cover slips were treated with benzophenone and rinsed with methanol as described in the previous section. Polyacrylamide pre-polymer mixture was sandwiched between two PDMS-coated coverslips and polymerized to produce hydrogel disks of 1 mm thickness. For control experiments, polyacrylamide gels on glass coverslips were prepared by replacing the PDMS coated coverslips with silane-treated glass coverslips, and polymerizing the hydrogel without UV light under a second Rain-X treated glass coverslip, following standard protocols.[41] The hydrogel disks were incubated in an excess volume of PBS at room temperature to swell overnight and to remove any unpolymerized monomers. Prior to measurements, excess PBS was dried off the top and bottom of the hydrogel disks and the sample was fixed between the rheometer plates using double-sided adhesive tape. Strain-controlled oscillatory tests between 1 and 10% were conducted, and data is reported as shear modulus (G) in kPa.

Table 1 Percentage of acrylamide and bisacrylamide used for preparation of different compositions of the hydrogel

Sample label	% acrylamide	% bis-acrylamide
PAAm-A	7.5	0.054
PAAm-B	7.6	0.236
PAAm-C	12	0.241
PAAm-D	16	0.96

2.4 Cell culture at air–liquid interface

Immortalized bronchial epithelial cells stably transduced with lentivirus containing wild-type cystic fibrosis transmembrane conductance regulator (CFBE41o-WT-CFTR; abbreviated as CFBEs in this manuscript) were used as an epithelial model for these demonstrative experiments. Cells were cultured in modified Eagle's medium (MEM) (Gibco, USA) supplemented with 10% fetal bovine serum (FBS), 1% anti–anti, 1% penicillin–streptomycin, and 2 mM L-glutamine, and maintained at 37 °C incubator in atmosphere of 5% CO_2. For the described experiments, the boats were transferred into appropriately-sized culture dishes with media. Neodymium rare earth magnets (K&J Magnetics Inc.; Pipersville, PA) were used as magnetic "anchors" to draw and hold the boat at the bottom of the dish (Fig. 2C). A suspension of trypsinized CFBE cells was seeded onto the collagen-coated polyacrylamide surfaces at a density of 2.5×10^5 cells per cm^2, which were kept submerged until they grew to confluence. Microboats were magnetically released from the bottom of the culture dish to remove culture media from the apical side and create ALI culture conditions. The culture medium on the basal side was replaced with an appropriate volume of fresh media every 24 h to sustain the ALI-cultured cells.

2.5 Trans-epithelial electrical resistance (TEER) measurements

To assess the formation of tight junctions and to evaluate the integrity of the epithelial barrier, we measured the trans-epithelial electrical resistance (TEER) of the epithelial monolayers formed on the polyacrylamide surface. TEER was measured using an epithelial volt–ohm-meter (EVOM2, World Precision Instruments) with chopstick electrodes (STX2, World Precision Instruments). The EVOM2 system was calibrated at steady state prior to making measurements. Prior to conducting the TEER measurements, the microboats were magnetically submerged and the medium was exchanged with pre-warmed medium. The system was then incubated at 37 °C for 10 minutes, which was empirically found to stabilize measured TEER values. TEER was measured by determining the resistance offered by the epithelial monolayer cultured on the polyacrylamide surfaces, and the measurements were made at 24 h intervals over 7 days. The measured resistance values were corrected for substrate resistance by subtracting the mean resistance of blank porous polyacrylamide membranes for the respective substrate stiffness. The final unit area resistance (Ω cm^2) was calculated by multiplying the resistance with the effective area of the porous membrane to obtain the TEER values for the epithelial cells, following standard practice.[42] TEER measurements were compared against standard Transwell culture membranes track-etched with 0.4 μm diameter holes (Corning C3470).

2.6 Immunofluorescent staining

Epithelial viability was assessed using a standard calcein AM/ethidium homodimer assay. Culture medium was replaced with 4 μM calcein-AM and 2 μM ethidium homodimer (EtHD) in PBS for 30 min. The medium was washed away and cultures were imaged. The formation of tight junctions between the epithelial cells were assessed by fluorescent labelling of the junction protein zonula occludens (ZO-1). Epithelial cells were fixed using a 4% paraformaldehyde in PBS for 20 minutes, and washed with PBS thrice for 5 minutes. The cells were then permeabilized using 0.1% Triton-X100 solution for 10 minutes at room temperature, and washed again with PBS. To decrease non-specific antibody binding, cells were incubated in a 2.5% blocking solution of goat serum in PBS at room temperature for 30 minutes. The serum was then replaced with a primary antibody at 1 : 50 dilution of ZO-1 monoclonal antibody (diluted in 2.5% goat serum, mouse host, Invitrogen 339100) overnight at room temperature. Cells were washed and incubated with the blocking buffer for 30 minutes, before incubation in a 1 : 1000 dilution of goat anti-mouse IgG (Abcam ab150116) secondary antibody tagged with Alexa Fluor 594 and diluted in 2.5% goat serum, for 1 hour at room temperature. Samples were then thoroughly washed in PBS, and cell nuclei were stained using a 2 μg ml^{-1} Hoechst 33258 (Invitrogen) in PBS for 30 minutes.

2.7 Nanoparticle toxicity assays

Copper(II) oxide nanopowder (Sigma Aldrich, 544868) with average particle size <50 nm was used in the experiments as a model toxic nanoparticle agent. The nanoparticle stock solutions were prepared by mixing the nanopowder in the culture medium, then diluted to the desired concentrations (1 μg mL^{-1}, 10 μg mL^{-1}, and 100 μg mL^{-1}) after syringe filtration through a 0.22 μm filter. After ALI culture, the basal culture medium was carefully replaced by nanoparticle-loaded media of varying concentrations. Assessment of junction formation was performed after 24 hours.

2.8 Imaging, analysis and statistics

Scanning electron microscopy (SEM, SU3500, Hitachi Hi-Technologies, Tokyo, Japan) was conducted using standard protocols for variable-pressure imaging mode (3.0 kV, 30 Pa,) which allowed SEM observations of cells on the hydrated hydrogels without the need for additional sample manipulation or conductive coating. Fluorescent microscopy was performed on an Olympus IX73 spinning disc confocal microscope. Microboats were placed directly on the microscope stage with a 20× long-working distance objective. For high resolution imaging (63×), fixed samples were dissected out of the boats and mounted on glass microscope coverslips. The formation of epithelial tight junctions under various experimental conditions was quantified manually in ImageJ (National Institute of Health, Bethesda, MD), following standard protocols,[43] in which the junction length was calculated as the total length of the fluorescent marker exhibiting classical cell–cell junction lines. All comparisons were made using one- or two-way ANOVA analyses with Tukey *post hoc* comparisons (Prism; GraphPad Software, La Jolla, CA) with p-values < 0.05

considered significant, and graphical data reported as means ± standard error for at least $n = 3$ experiments.

3. Results

3.1 Fabrication and microboat operation

The fabrication technique presented (Fig. 2) was successfully used to rapidly create dimensionally-consistent PDMS rings with embedded magnetic fibers, and with integrated stiffness-tunable polyacrylamide hydrogels using the described polyacrylamide grafting technique. As expected, microboats readily float at the liquid surface, and can be submerged on demand with the magnetic anchor. The magnetic fiber material used does not corrode or affect cultured cells, and was tested for up to 3 weeks in incubator conditions. We chose to colour-code our PDMS microboats based on formulation of the integrated hydrogel, which allows us to batch culture 'fleets' of floating microboats (Fig. 3A; shown in PBS for clarity), and separate them for individual experiments as needed (Fig. 3B). This colour-coding strategy may also be useful for studies of multiple cell types and treatment regimens. The microboats described in this manuscript have thicknesses of ~750 μm, with a 3 mm diameter culture area, and we empirically determined that devices with thickness to diameter ratios of greater than 0.5 were not sufficiently stable to avoid tipping or tumbling during the transition to ALI or standard handling. Hence, while larger ring sizes would be stable, smaller ring sizes may require a corresponding decrease in microboat thickness.

For individual cultures, each of the microboats can individually be submerged/released, using a small magnet (Fig. 3B). This may be important to precisely position individual microboats, as is needed in TEER measurements for example. Neodymium rare earth magnets generated a sufficient magnetic field to immerse the microboats when they floated on media at heights of ~10 mm, and removing the magnet allowed the boats to pop up to the liquid surface. Microboats could be submerged and released continuously and on demand, greatly simplifying the process of transitioning to ALI compared to traditional Transwell-type devices. Multiple

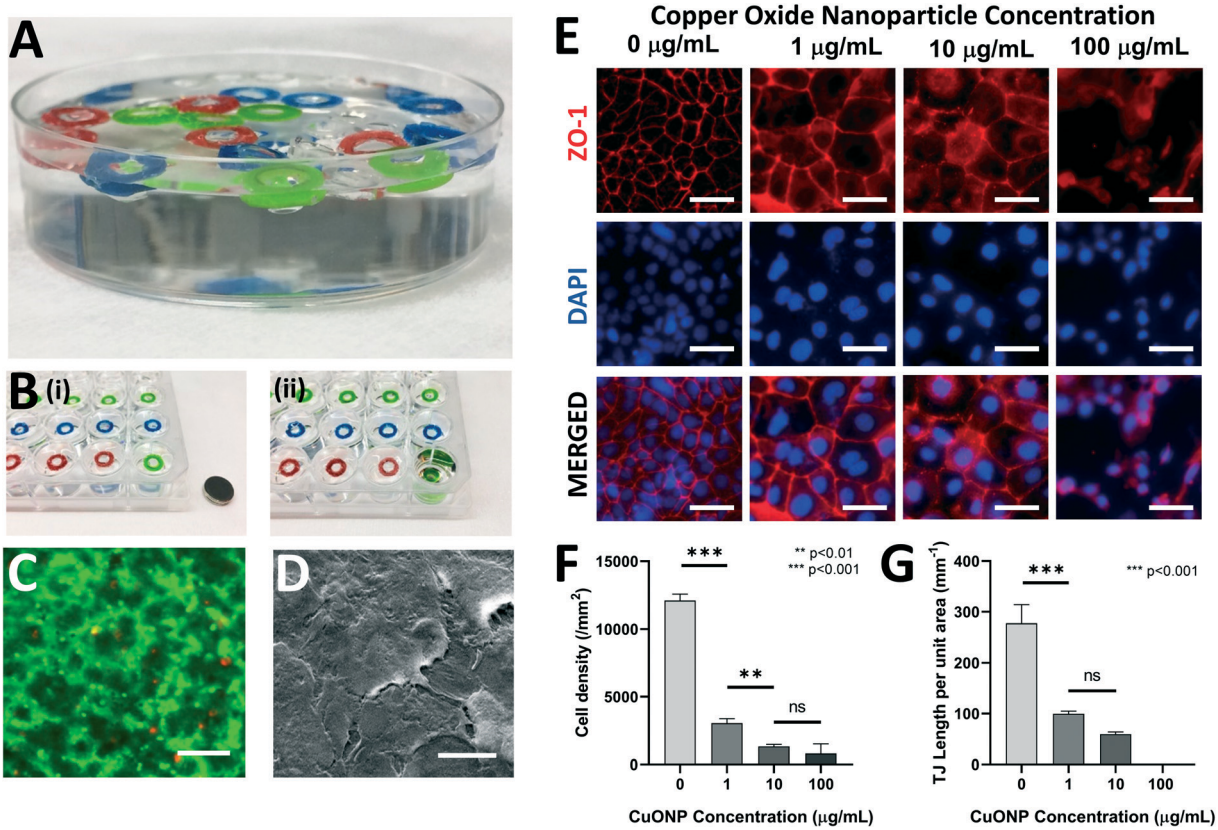

Fig. 3 Microboat operation and validation. (A) Demonstration of a fleet of hybrid, colour-coded, hydrogel-PDMS microboats floating at the air liquid interface in a culture dish (shown in PBS for clarity). (B) Microboats can be submerged by placing a strong neodymium magnet beneath the culture dish, and returned to air–liquid interface by removing the magnet. (C) CFBE cells are alive and adopt well-spread phenotypes after 24 h of ALI culture (green = live calcein AM marker; red = dead ethidium homodimer marker; scale bar = 125 μm). (D) Scanning electron micrograph of human bronchial epithelial cells after ALI culture on the floating microboats, demonstrating overlap and tight junctions between cells (scale bar = 15 μm). (E–G) Hydrogel matrices allow sufficient diffusion through their thickness to affect cell function, as evidenced by dose-dependent exposure responses to toxic copper oxide nanoparticles. (E) Fluorescent images of ALI-cultured epithelial cells after 24 hours of exposure to varying doses of copper oxide nanoparticles (CuONPs) in the underlying media (red = ZO-1 tight junction protein; blue = nuclear DAPI; scale bar = 50 μm). Cultures were quantified using (F) cell density and (G) tight junction length per unit area to demonstrate morphological and functional differences arising from nanoparticle exposure (**$p < 0.01$, ***$p < 0.001$, n.s. $p > 0.05$ by two-tailed ANOVA with Tukey *post hoc* comparisons; $n = 3$).

boats can also be simultaneously submerged/released for culture treatment or TEER measurements, with an array of small magnets beneath the culture vessel, or with a single sufficiently large magnet. Submersion and refloatation times were quite rapid and completed within 0.2 seconds (see Movie SM1†), but we did notice that the thin layer of liquid on the surface drains relatively slowly to establish. We hence quantified the time taken to achieve ALI conditions, and this was completed within 35 seconds of releasing the microboat magnetic anchor (Fig. S1†).

3.2 Microboats sustain air–liquid interface cultures

To demonstrate the biological capability of this platform, we cultured CFBEs on the microboats initially under submerged conditions, and then at ALI. The softest polyacrylamide hydrogel formulations were used for these initial experiments. CFBEs attached well to the collagen-coated polyacrylamide surfaces, and their morphologies were characterized by variable-pressure SEM. Sparsely-seeded cells were initially rounded in submerged culture, but displayed a classic spread morphology after culture at ALI (Fig. S3†). When cells were seeded at a high density of 2.5×10^5 cells per cm^2, the cells reached confluence within 24 hours of submerged culture. Subsequent culture at an ALI for 24 hours, and a standard live/dead stain demonstrates that over 99% of the cells on the polyacrylamide hydrogels were alive (Fig. 3C), demonstrating that nutrient transport through the polyacrylamide hydrogel is sufficient to sustain cells. Cells that initially grew on the PDMS surface rapidly died during ALI culture, and were washed away during submersion. SEM images reveal that even at this early time point of ALI culture, confluent cells began to form tight junctions with overlapping edges on the polyacrylamide surfaces (Fig. 3D). These results are consistent with previous findings for cultures of airway cells at ALI in Transwell dishes.[44] For both ALI and submerged culture conditions, no differences were observed in epithelial morphology for cultures in simple PDMS rings and in the modified microboat designs that were used to facilitate TEER measurements (Fig. S2†).

The hydrogels used in this work are substantially thicker than standard Transwell membranes, albeit significantly more porous and permissive to diffusion. Hence, it is uncertain whether they provide sufficient diffusive transport of molecules to support and stimulate cell culture, beyond the small-molecule metabolite exchanges needed to maintain cell viability at the ALI (as shown in Fig. 3C). To confirm whether the ~750 μm thick hydrogel layer allowed sufficient transport of larger molecules that might affect the cultured cells, we assessed whether cells respond to large macromolecular agents with known toxic effects, when carefully loaded into the underlying liquid media. Copper oxide nanoparticles (CuONPs) are generated by a wide variety of emerging technologies,[45] and although little is known of the *in vivo* activity of these particles on the lung epithelium,[46] *in vitro* studies have demonstrated significant respiratory epithelial damage arising from particle exposure.[47] CuONPs are commercially available with relatively large particle sizes of 50 nm, are virtually insoluble in water,[48] and the limited number of solubilized Cu^{2+} ions would be quickly chelated with serum albumin in the culture media. Since the hydrodynamic diameter of 50 nm particles is substantially greater than that of most large bioactive compounds, any effects on cultured cells would demonstrate sufficient diffusion through the hydrogel matrix. Hence, CuONPs were selected, and carefully loaded at concentrations of 0, 1, 10, and 100 μg mL^{-1} into the underlying liquid media for a 24 hour culture time period (Fig. 3E–G).

To measure epithelial impact during this assay, quantifying live/dead status was not sufficient, as dead cells tend to detach from the substrate, biasing the perceived viability of the cultures. Instead, we analyzed cell density (Fig. 3F) and demonstrated that, as expected, the number of cells remaining on the hydrogel after 24 hours of culture with CuONPs at ALI was significantly reduced when loading 1 μg mL^{-1} of nanoparticles into the underlying culture media. This effect increased in a dose-dependent manner. To assess formation of the epithelium in terms of functional markers, we analyzed the spatial expression of zonula occluden (ZO)-1, a tight junction protein that indicates appropriate formation of the epithelium. Sharp networks of ZO-1 formed between cells are hallmarks of epithelial ALI cultures[49] and the formation of these networks was disrupted by the CuONPs. To quantify this effect, we measured the total junction length per unit area, a previously validated metric for ZO-1 network analysis,[43] and demonstrated statistically significant disruptions to the ZO-1 network with increasing CuONP dosage. These results confirm and validate the potential capacity of this platform to grow and stimulate cells through the underlying basal support hydrogel.

3.3 Characterizing polyacrylamide hydrogels in the microboats

Polyacrylamide hydrogels are readily tunable by altering the hydrogel composition. Gels with expected stiffness of $G = 0.9$ to 12 kPa were successfully integrated onto the PDMS surfaces, using benzophenone-initiated surface grafting.[40] The hydrogels were strongly attached to the PDMS surfaces and could not be physically removed without tearing the gels. Some swelling of the gels did occur during the first 24 hours after polymerization, but this effect was minimal and only noticeable on the softest hydrogel formulation tested. This parameter should be carefully characterized for softer hydrogels, and may limit the size of the desired microboat to avoid swelling beyond the microscope imaging plane. Surface functionalization produced uniform coatings of collagen, as assessed by immunofluorescent staining for collagen I (data not shown). Polyacrylamide has been thoroughly characterized to have a stable linear elastic regime over a wide range of cell-generated strains, with minimal loss modulus,[50,51] but modifying polyacrylamide gels with the benzophenone grafting agent and polymerizing them in proximity to oxygen-rich PDMS warranted additional characterization, as oxygen

is known to influence polyacrylamide polymerization rates and therefore hydrogel mechanics.[51] The storage modulus for the different polyacrylamide compositions presented in Table 1 confirms distinct and relatively constant stiffnesses over the expected cell-generated deformations of 5% for polyacrylamide (Fig. 4A). Because slight variations were observed in the PAAm-D formulations across these strains, a larger range was tested for all samples, and PAAm-D formulation only showed an elevated loss modulus (Fig. S4†). For all other formulations, no appreciable loss modulus or non-linear stiffening behavior was observed.

To determine whether the grafting process itself changed the mechanics of the resulting hydrogel, we compared moduli values obtained from composite polyacrylamide-PDMS devices to the same polyacrylamide formulations polymerized on silane-activated glass coverslips (Fig. 4B). Unexpectedly, softer hydrogels stiffened by as much as a factor of 2× when grafted onto PDMS, and this effect decreased with stiffer hydrogels. This stiffening is likely due to differing organization and arrangement of the internal polyacrylamide microstructure, because the polymerization reaction is initiated at the PDMS surface, as well as within the bulk hydrogel material. These differences should be considered carefully when crosslinking polyacrylamide to PDMS.

For cell culture at ALI, sufficient hydrogel porosity is essential for basal nutrient or waste transport to maintain long-term cultures.[52] Polyacrylamide hydrogels of increased stiffness have increased crosslinking density, which could reduce the pore sizes of the network.[53] To further confirm that hydrogels allow comparable transport to standard techniques, we compared area-normalized TEER measurements between hydrogel boats and Transwells commonly used for ALI culture of CFBEs (Fig. 4C). No significant differences were observed in TEER between these cultures, and we therefore conclude that hydrogels of all stiffnesses present sufficient porosity to allow appropriate experimental comparison. These findings are consistent with previous studies demonstrating that polyacrylamide gels stiffer than 1 kPa have relatively minor changes in pore sizes.[53]

Finally, to verify that our stiffest hydrogels allow sufficient large-molecule transport for cell stimulation, we repeated our previous nanoparticle toxicity experiments (Fig. 3E–G) with the stiffest formulations (PAAm-D) identified here. We observed that even at the highest hydrogel crosslinking densities tested, cells exhibit similar responses to diffusing nanoparticles (Fig. S5†), demonstrating that the hydrogel network does not provide an appreciable diffusion barrier for these studies.

3.4 Epithelial phenotype at ALI is a function of substrate stiffness

Various respiratory diseases, such as CF, asthma, and COPD, are accompanied by abnormal epithelial permeability[54] and also exhibit altered ECM stiffness.[55] Since these diseases also feature impaired epithelial regeneration or healing after epithelial insult,[56] we reasoned that substrate stiffness may also influence the formation of an epithelial barrier at ALI conditions. To test this hypothesis, we cultured cells on microboats with stiffness-tunable substrates for 7 days at ALI, and monitored the formation of the epithelial barrier *via* routine TEER measurements during the experimental time course, and end-point staining for epithelial cell density, morphology and ZO-1 tight junction markers.

For each substrate stiffness tested, TEER was measured over the first 7 days of ALI culture (Fig. 5A). Although numerical TEER values vary significantly between cell type, passage number, and culture conditions based (as reviewed in ref.

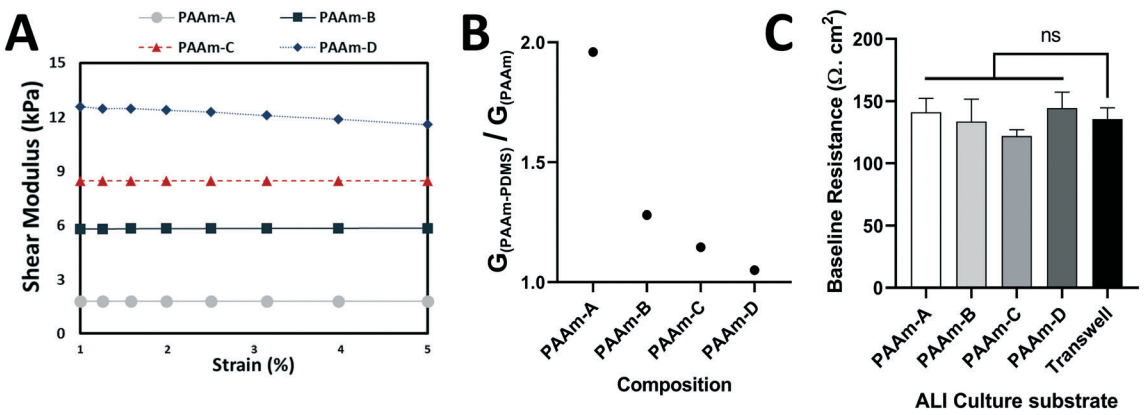

Fig. 4 Characterization of the four hydrogel formulations used in these experiments. (A) Shear modulus of the PDMS-integrated polyacrylamide hydrogels as assessed by shear rheometry. These findings suggest linear elasticity over the range of strains typically generated by cells in these experiments, and the ability to tune hydrogel stiffness across a range relevant to disease conditions. (B) Comparison of shear modulus values between polyacrylamide networks form *via* benzophenone photo-grafting on PDMS surfaces (PAAm-PDMS) and polyacrylamide networks formed on glass coverslips using standard techniques. As hydrogel networks contain more polyacrylamide content, observed variations between the two methods decrease. (C) Comparison of baseline electrical resistance measurements assessed by trans epithelial electrical resistance (TEER), between standard Transwells and hydrogel formulations used in this work. No significant differences were observed (n.s. $p > 0.05$ as assessed by two-tailed one-way ANOVA with Tukey *post hoc* comparisons, $n = 3$).

11), they often reach a peak value as the epithelium forms a tight barrier, depending on cell type and culture time.[57–60] In this work, cells were initially seeded at the same density, but softer substrates (1.8 and 5.8 kPa) caused a TEER peak within 48–72 hours of ALI culture. In contrast, epithelia on stiffer substrates (8.5 and 11.9 kPa) did not demonstrate significant variation in TEER values within 7 days of culture. Although the specific downstream effects of attaining a TEER peak is unknown, TEER does provide a lumped measure of multiple internal cellular processes, and peak TEER values hence represent a distinct set of processes that occurs at early time points on soft substrates, but not on stiff ones. We speculate that this could indicate the formation of functionally tight paracellular junctions between cells (decreased transport/increased resistance), which then mediates enhanced transcellular transport mechanisms (increased transport/decreased resistance). By the end of day 7, TEER values stabilized at ~100 Ω cm^2 over the baseline substrate resistance for all culture conditions. These results demonstrate the technical capacity of the microboat culture system to repeatedly switch between submerged and ALI cultures, and the measurements suggest that softer substrates could initiate the formation of functionally tight junctions more rapidly than stiff substrates, consistent with the idea that increased stiffness in diseased tissues may play a role in limiting the regenerative ability of the epithelium.

Given that TEER measurements are not always reliable measurements of barrier integrity,[61] we also conducted endpoint fluorescent analyses of epithelial morphology and markers of tight junction formation. Cells grown on softer substrates are significantly more densely packed (Fig. 5C) than those on stiffer substrates, with a corresponding significant decrease in projected nuclear area (Fig. 5D). On stiffer substrates, CFBEs adopt more well-spread cell and nuclear morphologies, consistent with several other studies demonstrating increased epithelial spread area with substrate stiffness.[32,62,63] These simple characteristics have broad impact on epithelial cell behaviour, given the well-established importance of cell and nuclear morphology on critical cell functions including apoptosis,[64] differentiation,[65] epithelial–mesenchymal transition,[66] transfection,[67] and various fundamental processes that occur during developmental, homeostatic, and pathological conditions.[68] Changes in cell shape and density were also accompanied by a dramatic change in ZO-1 network formation with increasing substrate stiffness (Fig. 5B). To quantify these differences, we examined

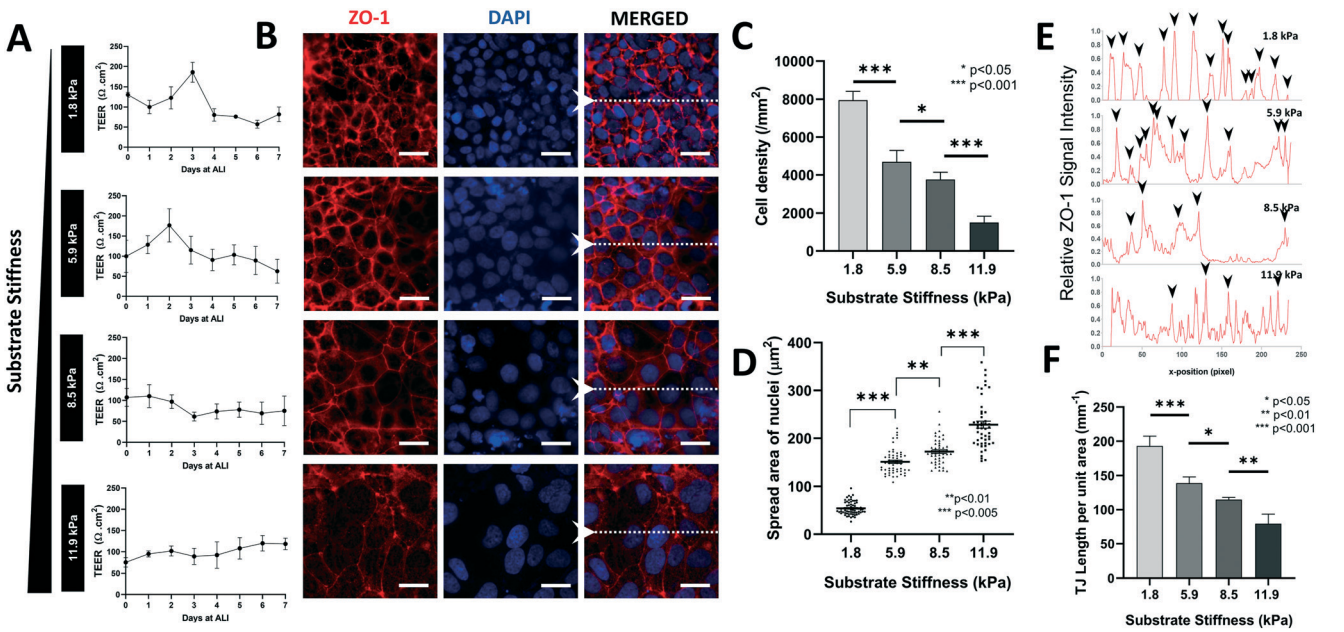

Fig. 5 Substrate stiffness influences epithelial phenotype during ALI culture. (A) TEER was measured across cells cultured at ALI over 7 days on four polyacrylamide formulations with nominal shear moduli of 1.8, 5.9, 8.5 and 11.9 kPa, representing the range of healthy *vs.* diseased lung matrix mechanics. Characteristic peaks for TEER were observed within 2 to 3 days in the 1.8 and 5.9 kPa culture conditions, but not in stiffer conditions (data presented as mean ± standard error for n = 3 samples). (B) Immunofluorescent characterization of epithelial cells after 7 days of culture at ALI demonstrates a well-developed network of tight junctions (ZO-1, red) with densely packed cells (Hoechst nuclear stain, blue) on soft substrates (scale bar = 25 μm). Metrics to quantify these findings included (C) cell density and (D) nuclear spread area, which demonstrate significant changes in cell morphology as a function of substrate stiffness. (E) Line intensity of normalized ZO-1 intensity is plotted for representative lines (shown as white dashed line in panel B). Black arrowheads indicate the expected positions of cell–cell junctions identified in the fluorescent images. Clear peaks are observed at these locations on softer substrates, but the signal grows more diffuse, and with fewer well-defined peaks on stiffer substrates. (F) Tight junction length measured per unit area is significantly reduced with increasing substrate stiffness. (Data presented for a minimum of n = 3 experiments, and minimum n = 50 for single cell measurements presented in panel D; and presented as mean ± standard error, with $*p < 0.05$, $**p < 0.01$, $***p < 0.001$, using two-tailed one way ANOVA, with Tukey *post hoc* comparisons).

the relative line intensity of ZO-1 expression across fluorescent images (Fig. 5E, using sample lines shown in Fig. 5B). Black arrowheads are used to indicate positions of cell-to-cell junctions identified visually using the fluorescent images. Cells cultured on the softest substrates demonstrate sharp peaks in ZO-1 intensity at expected locations based on cell position. Increasing substrate stiffness results in greater background intensity between expected peaks, as well as several peaks that are not associated with cell-to-cell junctions. Taken together, these results demonstrate that increases in substrate stiffness regulates the formation of the epithelial barrier during ALI culture, strongly suggesting that substrate stiffness should be considered as an important parameter in developing these culture systems.

4. Discussion

Air–liquid interface (ALI) is a required component of many lung cell culture protocols used to construct models of human respiratory tissue. Unfortunately, ALI culture can present significant handling challenges, particularly when physically manipulating mechanically delicate substrates such as soft hydrogels, or for repeated transitions between submerged and ALI culture necessary for routine monitoring and treatment of some cultures. This is relevant in studies aimed at understanding how cells interact with mechanical features in their surroundings, which may have considerable implications in designing next-generation drug discovery or disease modelling platforms that capture these essential elements of disease-specific microenvironments. Despite several recent efforts to include natural hydrogels such as collagen and Matrigel in microfluidic formats,[18,19,69] synthetic hydrogels with precisely-defined mechanical properties cannot be easily incorporated into microfluidic organ-on-a-chip culture formats.

To address these issues, we developed a hybrid hydrogel-PDMS floating "lung-on-a-boat" culture system that readily allows cell culture on stiffness-tunable polyacrylamide hydrogels maintained at ALI. The magnetically 'sinkable' microboats allow easy submersion and return to ALI *via* non-contact handling, as and when required by the study protocol. This technical innovation minimizes liquid handling inconsistencies, epithelial damage, and sample loss that frequently occurs when pipetting. Furthermore, the supporting hydrogel matrices present no significant diffusive barrier to soluble factors needed to maintain and stimulate epithelial cultures, confirming the utility of this microboat design. This concept of using microengineered boat-like structures may hence present significant practical advantages for scaled-up high-throughput needs of drug discovery and precision medicine. Furthermore, as a proof-of-concept, we demonstrate that substrate stiffness can modulate transepithelial barrier formation, suggesting that matrix mechanics is an important parameter that should be considered when designing these models. These results emphasize the need to integrate mechanically-tunable materials such as hydrogels into lung culture devices, and for technological platforms that can handle the increased experimental throughput requirements of such studies.

There are a few primary limitations to this platform in the current proof-of-concept format. First, although the described fabrication method used to prototype the PDMS rings is cost-effective, easy to implement, and allows rapid experimentation with simple structures, they do require a few intermediate manual handling steps, and are hence challenging to scale towards high-throughput experimentation. Simple modifications may be applied to increase fabrication throughput, further miniaturize the vessels, or simplify TEER analyses, as would be necessary in higher-throughput experiments. For example, magnetic microparticles can be blended with the PDMS directly to avoid the need for a magnetic fiber. High-volume and miniaturized production should also be possible with silicone rubber injection molding techniques, or using a guillotine-like microtome on an extruded silicone tube. PDMS rings can then be batch-filled with the desired polyacrylamide formulation by submerging the structures in pre-polymerized hydrogel and squeezing them between non-adhesive glass plates during polymerization. Similarly, low density particles may be added to the PDMS to optimize boat stability. Although we currently need a more complex microboat structure to simplify the TEER measurements (Fig. S2†), this may ultimately be performed directly on simple ring-like boats by designing an appropriate magnetic clamping system to electrically isolate the upper and lower compartments during the measurement. Similarly, weak magnetic traps may also be used to position the boats at ALI, and when combined with fluidic infrastructure could ultimately be used to analyze, sort, and screen cultures in a continuous flow process. Such a system could have significant advantages over conventional "solid" robotic systems for high-throughput screening.

Second, matrix stiffness has emerged as a critically important parameter in tissue engineering, and in understanding disease progression in biological systems. The effects of matrix stiffness on several biological systems, including the permeability of an endothelial cell layer barrier has been previously established,[70–72] but little is known about the effects of substrate stiffness on epithelial cells cultured at ALI. Our experiments demonstrate that the formation of barrier functions in an epithelium at ALI such as TEER measurements and ZO-1 patterns of spatial expression are dependent on substrate stiffness. However, the underlying mechanisms for this behaviour remain unknown. To thoroughly establish the mechanobiological response profile of lung cell cultures, these experiments must be conducted in a wide variety of epithelial primary and immortalized cell lines, and with appropriate inhibition or knock-down experiments to establish the relevant mechanosensitive signaling pathways, for both paracellular and transcellular transport mechanisms, and this platform presents an accessible method for such studies.

Third, the polyacrylamide hydrogel materials system presents several advantages including porosity, reproducibility, cost effectiveness, and surface customizability, as the

hydrogel surface can be functionalized with a wide variety of biomolecules using well-developed surface functionalization chemistries.[41] Mechanically, polyacrylamide is linear and elastic over several orders of magnitude, which allows for precisely-defined conditions for cell culture. However, the relatively recent development of tunable stress-relaxing hydrogels[73] has demonstrated that control over simple linear elastic mechanical properties is not sufficient to recapitulate the mechanically dynamic environment in the body,[22] which is now known to have a significant impact on cell function.[74] Integrating these advanced polymers into PDMS devices would require novel chemistries and device designs.

Finally, this submersible platform is not immediately suited to studies that integrate other microenvironmental parameters, such as mechanical stretch due to breathing in alveolar-scale lung cultures,[75] geometric curvature of the culture surface[76] that may play a role in higher generations of the branching respiratory tree, or advanced insult mechanisms such as alveolar collapse[77] or liquid plug rupture.[78] For models of tissue closer to the bronchi and bronchioles in the respiratory tree however, mechanical stretch and geometric curvature are not considered important parameters. Since these regions of the lung are primary interaction sites with inhaled respiratory drugs or environmental contaminants, developing high-throughput, easily-handled, and mechanically-realistic approaches is of critical importance for future studies; and the simple culture strategy developed here provides a versatile, accessible, defined and potentially scalable approach for such experiments.

Conclusions

We leveraged a novel strategy to establish an untethered, stiffness-tunable epithelial cell culture platform that can be transitioned between submerged and air–liquid interface culture conditions, in a reliable and reproducible manner. Magnetic buoyant microboats can be submerged on demand and released to rapidly establish ALI at the device surface. We confirmed that stiffness-tunable polyacrylamide hydrogels can be tightly integrated into the PDMS device architecture, and that functionalized hydrogels support culture of epithelial cells during ALI. We further confirmed that mass transport across the basal hydrogel supporting layer is sufficient to maintain and stimulate cultures over a range of substrate stiffnesses that mimic the linear elastic mechanical properties of healthy and diseased lung tissue. As a proof-of-concept experiment, we demonstrate that establishing epithelial barrier morphology and functionality at ALI is influenced by mechanics of the underlying substrate, which may be a novel microenvironmental parameter that limits recovery in progressive disease situations. More generally, the proposed culture strategy explores and presents a novel and versatile strategy that may be adapted to address the needs for high-throughput, physiologically-realistic, and precisely-defined tools to study respiratory disease.

Author contributions

AC, SK, JWH and CM conceptualized and designed the experiments. AC, SK, WL, NL, ZM and MJT conducted the experimental investigation. AC, SK, and ZM analyzed data. AC, JWH and CM wrote the original draft of this manuscript. All authors contributed to review and editing of the manuscript.

Conflicts of interest

There are no conflicts of interest to declare.

Acknowledgements

The authors would like to acknowledge Julie Goepp from the Hanrahan lab for valuable discussions. This project was funded by the Natural Sciences and Engineering Research Council of Canada (NSERC; Discovery RGPIN-2015-05512), FRQNT Team grant (205292), E-rare program sponsors: CF Canada (#3292), CIHR (ERT-144207) and FRQ-S (#34577), and the Canada Research Chair in Advanced Cellular Microenvironments to CM.

References

1 N. Hirota and J. G. Martin, *Chest*, 2013, **144**, 1026–1032.
2 R. C. Boucher, M. R. Knowles, M. J. Stutts and J. T. Gatzy, *Lung*, 1983, **161**, 1–17.
3 D. F. Rogers, *Pulm. Pharmacol. Ther.*, 2005, **18**, 1–8.
4 M. Loxham, D. E. Davies and C. Blume, *Clin. Exp. Allergy*, 2014, **44**, 1299–1313.
5 J. E. Nichols, J. A. Niles, S. P. Vega and J. Cortiella, *Stem Cell Res. Ther.*, 2013, **4**, S7.
6 A. J. Miller and J. R. Spence, *Physiology*, 2017, **32**, 246–260.
7 P. Chandorkar, W. Posch, V. Zaderer, M. Blatzer, M. Steger, C. G. Ammann, U. Binder, M. Hermann, P. Hörtnagl, C. Lass-Flörl and D. Wilflingseder, *Sci. Rep.*, 2017, **7**, 11644.
8 A. A. Pezzulo, T. D. Starner, T. E. Scheetz, G. L. Traver, A. E. Tilley, B.-G. Harvey, R. G. Crystal, P. B. McCray and J. Zabner, *Am. J. Physiol.*, 2010, **300**, L25–L31.
9 S. Upadhyay and L. Palmberg, *Toxicol. Sci.*, 2018, **164**, 21–30.
10 K. A. Moutasim, M. L. Nystrom and G. J. Thomas, in *Cancer Cell Culture: Methods and Protocols*, ed. I. A. Cree, Humana Press, Totowa, NJ, 2011, pp. 333–343.
11 B. Srinivasan, A. R. Kolli, M. B. Esch, H. E. Abaci, M. L. Shuler and J. J. Hickman, *J. Lab. Autom.*, 2015, **20**, 107–126.
12 R. A. Sheller, M. E. Cuevas and M. C. Todd, *Biol. Proced. Online*, 2017, **19**(1), 4.
13 D. D. Nalayanda, C. Puleo, W. B. Fulton, L. M. Sharpe, T.-H. Wang and F. Abdullah, *Biomed. Microdevices*, 2009, **11**, 1081–1089.
14 D. Huh, B. D. Matthews, A. Mammoto, M. Montoya-Zavala, H. Y. Hsin and D. E. Ingber, *Science*, 2010, **328**, 1662–1668.
15 X. Yang, K. Li, X. Zhang, C. Liu, B. Guo, W. Wen and X. Gao, *Lab Chip*, 2018, **18**, 486–495.
16 K. L. Sellgren, E. J. Butala, B. P. Gilmour, S. H. Randell and S. Grego, *Lab Chip*, 2014, **14**, 3349–3358.
17 C. Moraes, G. Mehta, S. C. Lesher-Perez and S. Takayama, *Ann. Biomed. Eng.*, 2012, **40**, 1211–1227.

18 M. Humayun, C.-W. Chow and E. W. K. Young, *Lab Chip*, 2018, **18**, 1298–1309.
19 M. J. Mondrinos, Y.-S. Yi, N.-K. Wu, X. Ding and D. Huh, *Lab Chip*, 2017, **17**, 3146–3158.
20 J. P. Soleas, T. K. Waddell and A. P. McGuigan, *Biomater. Sci.*, 2014, **3**, 121–133.
21 E. K. Sackmann, A. L. Fulton and D. J. Beebe, *Nature*, 2014, **507**, 181–189.
22 O. Chaudhuri, L. Gu, M. Darnell, D. Klumpers, S. A. Bencherif, J. C. Weaver, N. Huebsch and D. J. Mooney, *Nat. Commun.*, 2015, **6**, 6365.
23 A. J. Engler, S. Sen, H. L. Sweeney and D. E. Discher, *Cell*, 2006, **126**, 677–689.
24 D. E. Discher, P. Janmey and Y. Wang, *Science*, 2005, **310**, 1139–1143.
25 W. L. K. Chen and C. A. Simmons, *Adv. Drug Delivery Rev.*, 2011, **63**, 269–276.
26 H. Mohammadi and E. Sahai, *Nat. Cell Biol.*, 2018, **20**, 766.
27 N. Higuita-Castro, C. Mihai, D. J. Hansford and S. N. Ghadiali, *J. Appl. Physiol.*, 2014, **117**, 1231–1242.
28 E. S. White, *Ann. Am. Thorac. Soc.*, 2015, **12**, S30–S33.
29 C. Shimbori, J. Gauldie and M. Kolb, *Curr. Opin. Pulm. Med.*, 2013, **19**, 446–452.
30 D. J. Tschumperlin and J. M. Drazen, *Annu. Rev. Physiol.*, 2006, **68**, 563–583.
31 A. Shkumatov, M. Thompson, K. M. Choi, D. Sicard, K. Baek, D. H. Kim, D. J. Tschumperlin, Y. S. Prakash and H. Kong, *Am. J. Physiol.*, 2015, **308**, L1125–L1135.
32 J. L. Eisenberg, A. Safi, X. Wei, H. D. Espinosa, G. S. Budinger, D. Takawira, S. B. Hopkinson and J. C. Jones, *Res. Rep. Biol.*, 2011, **2011**, 1–12.
33 A. Brugués, E. Anon, V. Conte, J. H. Veldhuis, M. Gupta, J. Colombelli, J. J. Muñoz, G. W. Brodland, B. Ladoux and X. Trepat, *Nat. Phys.*, 2014, **10**, 683–690.
34 S. C. Wei, L. Fattet, J. H. Tsai, Y. Guo, V. H. Pai, H. E. Majeski, A. C. Chen, R. L. Sah, S. S. Taylor, A. J. Engler and J. Yang, *Nat. Cell Biol.*, 2015, **17**, 678–688.
35 F. Liu, J. D. Mih, B. S. Shea, A. T. Kho, A. S. Sharif, A. M. Tager and D. J. Tschumperlin, *J. Cell Biol.*, 2010, **190**, 693–706.
36 W. Guo, M. T. Frey, N. A. Burnham and Y. Wang, *Biophys. J.*, 2006, **90**, 2213–2220.
37 M. S. Hutson, J. Veldhuis, X. Ma, H. E. Lynch, P. G. Cranston and G. W. Brodland, *Biophys. J.*, 2009, **97**, 3075–3085.
38 J. T. Emerman and D. R. Pitelka, *In Vitro*, 1977, **13**, 316–328.
39 A. Marinković, F. Liu and D. J. Tschumperlin, *Am. J. Respir. Cell Mol. Biol.*, 2012, **48**, 422–430.
40 C. S. Simmons, A. J. S. Ribeiro and B. L. Pruitt, *Lab Chip*, 2013, **13**, 646.
41 J. R. Tse and A. J. Engler, in *Current Protocols in Cell Biology*, ed. J. S. Bonifacino, M. Dasso, J. B. Harford, J. Lippincott-Schwartz and K. M. Yamada, John Wiley & Sons, Inc., Hoboken, NJ, USA, 2010.
42 H. E. Nilsson, A. Dragomir, L. Lazorova, M. Johannesson and G. M. Roomans, *Exp. Mol. Pathol.*, 2010, **88**, 118–127.
43 C. M. Van Itallie, J. Holmes, A. Bridges, J. L. Gookin, M. R. Coccaro, W. Proctor, O. R. Colegio and J. M. Anderson, *J. Cell Sci.*, 2008, **121**, 298–305.
44 J. Wu, Y. Wang, G. Liu, Y. Jia, J. Yang, J. Shi, J. Dong, J. Wei and X. Liu, *Braz. J. Med. Biol. Res.*, 2017, **51**, e6950.
45 M. Grigore, E. Biscu, A. Holban, M. Gestal and A. Grumezescu, *Pharmaceuticals*, 2016, **9**(4), 75.
46 M. Ahamed, M. J. Akhtar, H. A. Alhadlaq and S. A. Alrokayan, *Nanomedicine*, 2015, **10**, 2365–2377.
47 B. Fahmy and S. A. Cormier, *Toxicol In Vitro*, 2009, **23**, 1365–1371.
48 D. A. Palmer, P. Bénézeth and J. M. Simonson, Solubility of copper oxides in water and steam, In *14th International Conference on the Properties of Water and Steam in Kyoto*, 2004, pp. 491–496.
49 E. McNeil, C. T. Capaldo and I. G. Macara, *Mol. Biol. Cell*, 2006, **17**, 1922–1932.
50 R. J. Pelham and Y. Wang, *Mol. Biol. Cell*, 1999, **10**, 935–945.
51 W. Lee, N. Kalashnikov, S. Mok, R. Halaoui, E. Kuzmin, A. J. Putnam, S. Takayama, M. Park, L. McCaffrey, R. Zhao, R. L. Leask and C. Moraes, *Nat. Commun.*, 2019, **10**(1), 144.
52 N. Annabi, J. W. Nichol, X. Zhong, C. Ji, S. Koshy, A. Khademhosseini and F. Dehghani, *Tissue Eng., Part B*, 2010, **16**, 371–383.
53 B. Trappmann, J. E. Gautrot, J. T. Connelly, D. G. T. Strange, Y. Li, M. L. Oyen, M. A. C. Stuart, H. Boehm, B. Li, V. Vogel, J. P. Spatz, F. M. Watt and W. T. S. Huck, *Nat. Mater.*, 2012, **11**, 642–649.
54 M. Aghapour, P. Raee, S. J. Moghaddam, P. S. Hiemstra and I. H. Heijink, *Am. J. Respir. Cell Mol. Biol.*, 2018, **58**, 157–169.
55 J. K. Burgess, T. Mauad, G. Tjin, J. C. Karlsson and G. Westergren-Thorsson, *J. Pathol.*, 2016, **240**, 397–409.
56 M. Spella, I. Lilis and G. T. Stathopoulos, *Eur. Respir. Rev.*, 2017, **26**(144), 170048.
57 H. Tavana, P. Zamankhan, P. J. Christensen, J. B. Grotberg and S. Takayama, *Biomed. Microdevices*, 2011, **13**, 731–742.
58 H. Lin, H. Li, H.-J. Cho, S. Bian, H.-J. Roh, M.-K. Lee, J. S. Kim, S.-J. Chung, C.-K. Shim and D.-D. Kim, *J. Pharm. Sci.*, 2007, **96**, 341–350.
59 M.-K. Lee, J.-W. Yoo, H. Lin, Y.-S. Kim, D.-D. Kim, Y.-M. Choi, S.-K. Park, C.-H. Lee and H.-J. Roh, *Drug Delivery*, 2005, **12**, 305–311.
60 O. Y. F. Henry, R. Villenave, M. J. Cronce, W. D. Leineweber, M. A. Benz and D. E. Ingber, *Lab Chip*, 2017, **17**, 2264–2271.
61 T. Mukherjee, E. Squillantea, M. Gillespieb and J. Shao, *Drug Delivery*, 2008, **11**, 11–18.
62 J. Li, D. Han and Y. P. Zhao, *Sci. Rep.*, 2014, **4**, 3910.
63 K. M. Stroka, B. S. Wong, M. Shriver, J. M. Phillip, D. Wirtz, A. Kontrogianni-Konstantopoulos and K. Konstantopoulos, *Oncotarget*, 2016, **8**, 54004–54020.
64 C. S. Chen, M. Mrksich, S. Huang, G. M. Whitesides and D. E. Ingber, *Science*, 1997, **276**, 1425–1428.
65 K. A. Kilian, B. Bugarija, B. T. Lahn and M. Mrksich, *Proc. Natl. Acad. Sci. U. S. A.*, 2010, **107**, 4872.
66 E. W. Gomez, Q. K. Chen, N. Gjorevski and C. M. Nelson, *J. Cell. Biochem.*, 2010, **110**, 44–51.

67 H. J. Kong, J. Liu, K. Riddle, T. Matsumoto, K. Leach and D. J. Mooney, *Nat. Mater.*, 2005, **4**, 460–464.
68 K. N. Dahl, A. J. S. Ribeiro and J. Lammerding, *Circ. Res.*, 2008, **102**, 1307–1318.
69 B. P. Casavant, E. Berthier, A. B. Theberge, J. Berthier, S. I. Montanez-Sauri, L. L. Bischel, K. Brakke, C. J. Hedman, W. Bushman, N. P. Keller and D. J. Beebe, *Proc. Natl. Acad. Sci. U. S. A.*, 2013, **110**, 10111–10116.
70 A. Mammoto, T. Mammoto, M. Kanapathipillai, C. W. Yung, E. Jiang, A. Jiang, K. Lofgren, E. P. S. Gee and D. E. Ingber, *Nat. Commun.*, 2013, **4**, 1759.
71 P. Karki and A. A. Birukova, *Pulm. Circ.*, 2018, **8**(2), 2045894018773044.
72 J. A. VanderBurgh, H. Hotchkiss, A. Potharazu, P. V. Taufalele and C. A. Reinhart-King, *Integr. Biol.*, 2018, **10**, 734–746.
73 C. M. Madl, B. L. LeSavage, R. E. Dewi, C. B. Dinh, R. S. Stowers, M. Khariton, K. J. Lampe, D. Nguyen, O. Chaudhuri, A. Enejder and S. C. Heilshorn, *Nat. Mater.*, 2017, **16**, 1233–1242.
74 O. Chaudhuri, S. T. Koshy, C. Branco da Cunha, J.-W. Shin, C. S. Verbeke, K. H. Allison and D. J. Mooney, *Nat. Mater.*, 2014, **13**, 970–978.
75 O. T. Guenat and F. Berthiaume, *Biomicrofluidics*, 2018, **12**(4), 042207.
76 S.-M. Yu, J. M. Oh, J. Lee, W. Lee-Kwon, W. Jung, F. Amblard, S. Granick and Y.-K. Cho, *Acta Biomater.*, 2018, 77, 311–321.
77 N. J. Douville, P. Zamankhan, Y.-C. Tung, R. Li, B. L. Vaughan, C.-F. Tai, J. White, P. J. Christensen, J. B. Grotberg and S. Takayama, *Lab Chip*, 2011, **11**, 609–619.
78 D. Huh, H. Fujioka, Y. C. Tung, N. Futai, R. Paine, J. B. Grotberg and S. Takayama, *Proc. Natl. Acad. Sci. U. S. A.*, 2007, **104**, 18886–18891.